Split-Crank Functional Electrical Stimulation Cycling: An Adapting Admitting Rehabilitation Robot

Christian A. Cousin, *Member, IEEE*, Courtney A. Rouse,
and Warren E. Dixon, *Fellow, IEEE*

Abstract—Motorized functional electrical stimulation (FES) cycling is a promising rehabilitation strategy for individuals with movement disorders, particularly when the pedals of the FES cycle are decoupled to measure and address asymmetries. In this article, a rehabilitation robot, i.e., a split-crank FES cycle, is developed which utilizes a combined admittance-cadence controller to address rider asymmetries through adaptation, ensure rider safety, and electrically stimulate the rider's leg muscles to pedal the cycle at the desired cadence. The theoretical development of the controllers is based on a combined Lyapunov-passivity switched systems stability analysis. Experiments were conducted on one able-bodied participant and three participants with various movement disorders, resulting in an average admittance tracking error of -0.13 ± 1.77 RPM with adaptation and -0.03 ± 4.05 RPM without adaptation. The split-crank FES cycle successfully admits to the rider, preserves rider safety, and offers a promising robotic rehabilitation strategy for individuals affected by movement disorders.

Index Terms—Admittance, functional electrical stimulation (FES), Lyapunov, nonlinear control, rehabilitation.

I. INTRODUCTION

EVERY year, it is estimated that 2.5 million Americans experience a traumatic brain injury [1], 800 000 experience a stroke [2], and nearly 18 000 suffer a spinal cord injury [3]. Consequently, millions of Americans are left with permanent movement disorders from these neurological conditions (NCs) and others [1], [3]. NCs result from damage to the brain or spinal cord, and consequently, the muscles/nerves controlled by the damaged tissue become compromised and can result in a movement disorder, such as hemiparesis or paralysis [4].

In an effort to reduce the negative secondary consequences of movement disorders and improve the overall quality of life of individuals affected by NCs, numerous rehabilitation options are being investigated, namely, functional electrical stimulation (FES) and rehabilitation robots. While FES has been proven to improve muscle strength [5] and motor control [6], and rehabilitation robots have been shown to improve motor function [7], [8], both therapeutic options have their respective inherent challenges. For example, the nonlinear dynamics exhibited by muscles and time-varying characteristics, such as fatigue [9], compromise the accurate regulation of movement elicited by FES, and when a robot is physically coupled to a human, safety must be prioritized and incorporated into the robot's control structure.

When dealing with a physical human–robot interaction, a number of studies have employed various strategies to control robots. For example, Kimmel and Hirche utilized invariance control to enforce dynamic constraints and keep the robot in a safe configuration. Other studies have implemented a number of control modes for the robot to operate under, such as *assist-as-needed*, for upper limb rehabilitation robots [11], [12], *human-in-charge/force control mode* for use with series elastic actuators [11], and *patient-in-charge/robot-in-charge* modes for elbow rehabilitation [13]. Alternatively, Atashzar *et al.* provides a framework where a therapist can be injected into the control loop with the use of haptics-enabled telerobotic rehabilitation to provide resistive/assistive motor therapy remotely to stabilize nonpassive, nonlinear, and nonautonomous behavior.

Admittance control, pioneered by Hogan [15], is an additional control strategy capable of modifying robot behavior based on force-feedback and offers a method to promote safety over performance by resolving conflicts in motion between the robot and human [11]. Admittance control is also amenable to adaptive control methods, and previous results have integrated adaptation in the outer-loop of force-feedback to modify the admittance parameters [16], [17] or within the inner-loop to modify the position controller using techniques, such as neural networks [18]. While admittance control has been implemented on a number of rehabilitation robots [18]–[20] and hybrid exoskeletons (which combine FES with rehabilitation robots) [21], [22], subsets of admittance control, such as stiffness control [23], and extensions, such as dissipative

control [24] (i.e., admittance control with a minimum guarantee of passivity), have also been used to accomplish safe, stable human–robot interaction.

An example of hybrid exoskeletons (see [25], [26]) and the focus of this article is FES cycles, where the human rider is electrically stimulated and an electric motor is used to generate pedaling torques [27]. While objectives of FES cycling can include cadence [27] or torque tracking [28]–[30], admittance control strikes a balance between the two and has been implemented on FES cycles in the authors' preliminary works (see [31]–[34]). When dealing with hemiparesis, FES cycles can often mask asymmetries in the rider due to coupled pedals and a single-torque sensor, allowing the rider to "cheat" at the pedaling task by only utilizing their unimpaired side to pedal the cycle. Previous works have, thus, derived methods to promote symmetric rehabilitation by isolating the torque contributions of each leg by instrumenting cycles with torque sensors on each pedal [35], [36], decoupling the pedals (i.e., split-crank cycling) [37], [38], or pedaling with one leg at a time (i.e., one-legged pedaling) [39]. Results, such as [36], derived symmetry controllers and stimulate each leg differently to balance the contributions of each leg and promote rehabilitation outcomes. Because FES cycling has been shown to improve symmetry in hemiplegic individuals [35], further research into asymmetric rehabilitation is warranted.

Asymmetric rehabilitation is supported by numerous studies, such as [40], which indicated that children with unilateral brain injury have separate control circuits for each leg, and these circuits can be adapted independently to improve symmetry [41], which found that split-belt treadmills and individual limb weighting can improve spatiotemporal symmetry in poststroke adults, and [42], which demonstrated that decreases in asymmetry were observed in people with Parkinson's disease in cycling when the average workload increased. As a whole, the literature suggests that within various NCs resulting in hemiparesis, symmetry can be improved, at least in the short term, by targeted rehabilitation of the affected and nonaffected sides of the body. Moreover, motivation exists to have individuals participate in rehabilitation to the greatest extent possible in an effort to reduce neuromuscular impairment [20].

Split-crank FES cycling offers a method for asymmetric rehabilitation, but because it involves physically coupling a rehabilitation robot to the human rider, the numerous challenges of any physical human–robot interaction task (e.g., safety, closed-loop control, and nonlinearities) must be addressed. Furthermore, FES cycling has the added challenge of discretely switching muscle stimulation ON/OFF with continuously evolving state dynamics, resulting in a switched system, and requires a switched systems stability analysis to illustrate stability [43] and guarantee rider safety. Split-crank cycling is also highly susceptible to periodic torques (e.g., due to gravity), which are no longer balanced about the cycle's crankshaft due to decoupled pedals. Because people have different capabilities and every movement disorder is unique, adaptive control of FES cycling is warranted to not only account for cycle dynamics but also produce a customized experience for each rider while avoiding high-frequency switching in the control effort, typically found in robust control methods (e.g., sliding-mode control).

Motivated by the desire to promote rehabilitation in individuals with movement disorders, specifically hemiparesis, this article implements novel closed-loop adaptive admittance controllers on the decoupled motors of a split-crank FES cycle, while the rider is electrically stimulated with a robust cadence controller. Compared with the past literature and our previous work on admittance control of FES cycling (see [31]–[34]), this article provides the first instance of admittance control applied to a split-crank FES cycle with results on participants possessing NCs, a rigorous Lyapunov-like and passivity-based switched systems stability analysis, and a generalized framework to investigate numerous split-crank cadence/admittance trajectories using adaptive control. Furthermore, by instrumenting the FES cycle with sensors on each side, we are now able to measure the performance of each participant's right and left leg, allowing for an estimate of asymmetries.

Compared with other methods of control for hybrid exoskeletons or hybrid neuroprostheses, the current approach is capable of simultaneously regulating the dynamic interaction between the human and the robot (see [44], which utilized repetitive learning controllers to alternate the activation of motors and muscles for explicit cadence tracking); automatically and adaptively modulating the amount of motorized assistance in real time (see [25], which utilized an offline-computed optimal synergy-based feedforward component within the controller); and addressing time-varying trajectories (see [45], which utilized online optimization (MPC) for regulation tasks).

Because a few results exist in terms of split-crank cycling, open questions remain regarding how to best design the desired trajectories and select the appropriate admittance parameters. Although the development of this article is agnostic to the desired trajectories, various trajectories are hypothesized to have different clinical implications for people with movement disorders [46]. To allow further investigation into asymmetric rehabilitation, we developed a novel framework which can be used with a variety of trajectories and admittance filters. Without loss of generality, we selected the admitted trajectory to be generated from the average capabilities of the two sides of the split-crank FES cycle; that is, torque feedback is implemented on each side of the cycle and averaged, such that the more capable leg experiences resistance and the less capable leg experience assistance to achieve the same cadence and preserve cycling symmetry. A closed-loop robust cadence controller is subsequently designed to implement FES on the large muscle groups of the rider's legs (quadriceps, hamstrings, and gluteals) and maintain the desired cadence. To ensure rider safety, the combined closed-loop cycle-rider system is proven to be energetically dissipative (i.e., stable and passive). A Lyapunov-passivity-based stability analysis is used to prove the developed cadence controller is passive, and the admittance controller exhibits global asymptotic admittance tracking. The two controllers work in tandem to cooperatively pedal the split-crank FES cycle while promoting rehabilitation outcomes using a rehabilitation robot.

Experiments were conducted on one able-bodied participant, one participant with spina bifida, one participant with poststroke right-sided hemiparesis, and one participant with Parkinson's disease, with and without controller adaptation. An additional experiment was conducted on the participant with Parkinson's disease to evaluate the effect of adding rider volition to the experiment. To the best of our knowledge, this is the first instance of adaptive admittance control applied to split-crank FES cycling and, based on the experimental results, offers a promising strategy for safely controlling robots interacting with individuals affected by movement disorders.

II. DYNAMICS

Because the following analysis will be completed on a split-crank cycle and the cycle is symmetric by design, the dynamics are presented for a single side without loss of generality. The cycle-rider dynamics for one side of the FES cycle can be modeled by the uncertain, nonlinear, single-degree-of-freedom system[1,2]

$$\tau_m(q, \dot{q}, t) + \tau_e(t) = M(q)\ddot{q} + V(q, \dot{q})\dot{q} + G(q) \\ + P(q, \dot{q}) + b\dot{q} + d(t) \quad (1)$$

where $q : \mathbb{R}_{\geq 0} \to \mathcal{Q}$ denotes the measurable crank angle, $\mathcal{Q} \subseteq \mathbb{R}$ is a set which contains all possible crank angles, $\dot{q} : \mathbb{R}_{\geq 0} \to \mathbb{R}$ denotes the measurable velocity, and $\ddot{q} : \mathbb{R}_{\geq 0} \to \mathbb{R}$ denotes the nonmeasurable acceleration. The inertial, centripetal-Coriolis, and gravitational effects of the combined cycle-rider system are denoted by $M : \mathcal{Q} \to \mathbb{R}$, $V : \mathcal{Q} \times \mathbb{R} \to \mathbb{R}$, and $G : \mathcal{Q} \to \mathbb{R}$, respectively. The rider's passive viscoelastic tissue torques and the cycle's friction are denoted by $P : \mathcal{Q} \times \mathbb{R} \to \mathbb{R}$ and $b \in \mathbb{R}_{>0}$, respectively. Unmodeled system disturbances (e.g., unintended volitional efforts from the rider) are denoted by $d : \mathbb{R}_{\geq 0} \to \mathbb{R}$. The combined torque from the rider's muscles[3] is denoted by $\tau_m : \mathcal{Q} \times \mathbb{R} \times \mathbb{R}_{\geq 0} \to \mathbb{R}$ and the torque from the cycle's motor is denoted by $\tau_e : \mathbb{R}_{\geq 0} \to \mathbb{R}$, which can, respectively, be expanded as

$$\tau_m(q, \dot{q}, t) \triangleq \sum_{m \in \mathcal{M}} B_m(q, \dot{q})\sigma_m(q)u_h(t) \quad (2)$$

$$\tau_e(t) \triangleq B_e u_e(t). \quad (3)$$

The uncertain, nonlinear, individual muscle control effectiveness relates stimulation input to output torque and is denoted by $B_m : \mathcal{Q} \times \mathbb{R} \to \mathbb{R}_{>0}$ [9], [27], and the piecewise right-continuous switching signal for activating the individual muscle groups is denoted by $\sigma_m : \mathcal{Q} \to \{0, 1\}$, $\forall m \in \mathcal{M}$, where the set $\mathcal{M} \triangleq \{Q \, H \, G\}$ includes the quadriceps femoris (Q), hamstring (H), and gluteal (G) muscle groups (i.e., the stimulated muscle groups). The subsequently designed muscle control input is distributed to all muscle groups and is denoted by $u_h : \mathbb{R}_{\geq 0} \to \mathbb{R}$. This muscle control

input is used to construct a stimulation pulsetrain delivered to the rider's muscles with a fixed current amplitude and frequency, but variable pulsewidth (i.e., the parameter modulated by the subsequently designed controller u_h). The known motor control constant relating the motor's input current to output torque is denoted by $B_e \in \mathbb{R}_{>0}$, and the subsequently designed motor control current is denoted by $u_e : \mathbb{R}_{\geq 0} \to \mathbb{R}$. The switching signal σ_m is defined as [27]

$$\sigma_m(q) \triangleq \begin{cases} 1, & q \in \mathcal{Q}_m \\ 0, & q \notin \mathcal{Q}_m \end{cases} \quad (4)$$

$\forall m \in \mathcal{M}$, where $\mathcal{Q}_m \subset \mathcal{Q}$ denotes the regions in which muscle group m is able to supply a positive torque about the crank. The union of all muscle regions establishes the combined FES region of the crank cycle, defined as $\mathcal{Q}_M \triangleq \bigcup_{m \in \mathcal{M}} \mathcal{Q}_m$, and the kinematic deadzone (KDZ) region as the remainder. By appropriately designing the switching signals in (4), each muscle is stimulated only when it can effectively contribute to the tracking objective (i.e., when it can apply torque in the same direction as the control input u_h). To delay muscle fatigue, muscles are only stimulated when in kinematically efficient regions (i.e., at a high torque transfer ratio from muscle to crank) [27], [44]. As muscle fatigue does occur, however, the rider will receive an increasing amount of stimulation delivered to their leg muscle groups to evoke stronger muscle contractions due to the closed-loop nature of the controller in (2). Since different muscle groups are activated through their respective switching signals, the torque input to the system discretely changes; however, the system states continuously evolve. The combination of discretely changing control inputs with continuous state dynamics gives rise to a state-dependent switched system.

The switched system dynamics in (1) have the following properties [27].

Property 1: The dynamic parameters M, V, G, P, b, and d are bounded by $c_m \leq M \leq c_M$, $|V| \leq c_V|\dot{q}|$, $|G| \leq c_G$, $|P| \leq c_{P1} + c_{P2}|\dot{q}|$, $b \leq c_b$, $|d| \leq c_d$, where c_m, c_M, c_V, c_G, c_{P1}, c_{P2}, c_b, $c_d \in \mathbb{R}_{>0}$ are known constants.

Property 2: The uncertain dynamic terms M, V, G, and b are linear in the parameters [47].

Property 3: The system is skew symmetric by the relation $\dot{M} - 2V = 0$.

Property 4: The individual muscle control effectiveness, B_m, is subject to nonlinear activation dynamics and a muscle fiber recruitment curve (commonly represented by sigmoidal function) [48], [49]. However, when $q \in \mathcal{Q}_M$, the unknown muscle control effectiveness mapping the FES input to the output muscle force is bounded by $\underline{B_m} \leq \sum_{m \in \mathcal{M}} B_m \sigma_m \leq B_{\overline{m}}$, where $\underline{B_m}$, $B_{\overline{m}} \in \mathbb{R}_{>0}$ are known constants.

III. CONTROL DEVELOPMENT

In the following section, two controllers are developed for one side of the FES cycle: a sliding-mode cadence controller to stimulate the rider's muscles via FES and an adaptive sliding-mode admittance controller to activate the cycle's

---

[1]For notational brevity, all explicit dependence on time, t, within the states $q(t)$, $\dot{q}(t)$, and $\ddot{q}(t)$ is suppressed.

[2]Because each side of the FES cycle is a single-degree-of-freedom system, the terms representing the dynamics in (1) reduce to scalars.

[3]The torque arising from the rider's muscle is subject to an input delay [9] which is addressed in Section V-B.

motor; without loss generality, an identical analysis can be repeated for each side of the FES cycle.

A. Cadence Controller

As in [27], the cycle's cadence is regulated using the rider's muscles in the FES regions. The cadence tracking objective is quantified by a position error denoted by $e : \mathbb{R}_{\geq 0} \to \mathbb{R}$ and a filtered tracking error (combining both the position error and its derivative) denoted by $r : \mathbb{R}_{\geq 0} \to \mathbb{R}$, each defined as[4]

$$e \triangleq q_d - q \tag{5}$$
$$r \triangleq \dot{e} + \alpha e \tag{6}$$

where $q_d : \mathbb{R}_{\geq 0} \to \mathbb{R}$ denotes the desired position, designed to be sufficiently smooth (i.e., $q_d, \dot{q}_d, \ddot{q}_d \in \mathcal{L}_\infty$), $\alpha \in \mathbb{R}_{>0}$ denotes a constant control gain, and r acts as a sliding surface. The open-loop cadence error system is obtained by taking the derivative of (6), multiplying by M, adding and subtracting e, and substituting (1), (5), and (6) to yield

$$M\dot{r} = \chi - \sum_{m \in \mathcal{M}} B_m \sigma_m u_h - \tau_e - Vr - e \tag{7}$$

where the lumped auxiliary signal $\chi : \mathbb{R}^2 \times \mathbb{R}_{\geq 0} \to \mathbb{R}$ denoting system disturbances is defined as $\chi \triangleq M(\ddot{q}_d + \alpha r - \alpha^2 e) + V(\dot{q}_d + \alpha e) + G + P + b(\dot{q}_d - r + \alpha e) + d + e$ and bounded by Property 1 as $|\chi| \leq c_1 + c_2\|z\| + c_3\|z\|^2$, where $c_1, c_2, c_3 \in \mathbb{R}_{>0}$ are known constants, and the error vector $z \in \mathbb{R}^2$ is defined as $z \triangleq [e, \ r]^T$. Based on (7) and the subsequent stability analysis, the cadence controller is designed as

$$u_h \triangleq \text{sat}_\rho \left[\frac{1}{B_{\underline{m}}} \Big(k_1 r + \big(k_2 + k_3\|z\| + k_4\|z\|^2 \big) \text{sgn}(r) \Big) \right] \tag{8}$$

where $\text{sat}_\rho(\cdot)$ denotes the saturation function with saturation limit $\rho \in \mathbb{R}_{>0}$, $k_i \in \mathbb{R}_{>0} \ \forall i \in \{1, \ 2, \ 3, \ 4\}$ denote constant control gains, $\|\cdot\|$ denotes the standard Euclidean norm, $\text{sgn}(\cdot)$ denotes the signum function, and $B_{\underline{m}}$ is introduced in Property 4. Substituting (8) into (7) yields the closed-loop cadence error system

$$M\dot{r} = \chi - \tau_e - Vr - e - \sum_{m \in \mathcal{M}} B_m \sigma_m \text{sat}_\rho$$
$$\times \left[\frac{1}{B_{\underline{m}}} (k_1 r + (k_2 + k_3\|z\| + k_4\|z\|^2)\text{sgn}(r)) \right]. \tag{9}$$

B. Admittance Controller

While the rider's muscles regulate cadence, an admittance filter is employed to generate the admitted trajectory online; the filter is selected as

$$\tau - \tau_d \triangleq M_d \ddot{q}_a + B_d \dot{q}_a \tag{10}$$

where $\tau_d : \mathbb{R}_{\geq 0} \to \mathbb{R}$ denotes the desired bounded interaction torque, and $\tau : \mathbb{R}_{\geq 0} \to \mathbb{R}$ denotes the bounded measurable interaction torque between the cycle and rider (i.e., $\tau \in \mathcal{L}_\infty$) [10], [17]. The filter's parameters, represented by the desired inertial and damping constants $M_d, \ B_d \in \mathbb{R}_{>0}$, respectively,

---

[4]For notational brevity, all functional dependencies are hereafter suppressed unless required for clarity of exposition.

are selected such that the transfer function of (10) is passive [50, Lemma 6.4] (i.e., $q_a, \ \dot{q}_a \ \ddot{q}_a \in \mathcal{L}_\infty$), where $q_a, \ \dot{q}_a, \ \ddot{q}_a :$ $\mathbb{R}_{\geq 0} \to \mathbb{R}$ denote the generated admitted position, velocity, and acceleration, respectively.

The primary goal of the admittance controller is to promote rider safety by injecting dynamics of the form in (10) that relate the admitted trajectory to the desired trajectory. Therefore, while tracking the desired cadence, the most influential admittance parameter is the damping coefficient, B_d. Because damping is proportional to cadence, a higher damping coefficient results in a stiffer admitted cadence trajectory (which the motor tracks) and allows for less deviation from the desired cadence trajectory (which the rider tracks).

Moreover, the admitted cadence trajectory can be made more volatile by decreasing the desired inertia coefficient, M_d. Decreasing the inertia is analogous to removing mass from the system in that admitted trajectory is more susceptible to change. The admitted trajectory only evolves if there exists a nonzero value on the left side of (10); therefore, if the rider is able to generate exactly the desired interaction torque, the motor will not assist (or resist) the rider in maintaining the desired cadence trajectory. Only if the rider falls short of the desired interaction torque does the assist-as-needed control paradigm take effect. Conversely, if the rider exceeds the desired interaction torque (such as is possible in volitional pedaling), the cycle will enter a resist-as-needed paradigm to challenge the rider.

To track the admitted trajectory, an inner-loop position controller is designed to regulate the admittance error system. The admittance position error is denoted by $\xi : \mathbb{R}_{\geq 0} \to \mathbb{R}$, and a filtered tracking error denoted by $\psi : \mathbb{R}_{\geq 0} \to \mathbb{R}$, each defined as

$$\xi \triangleq \Xi + q_d - q \tag{11}$$
$$\psi \triangleq \dot{\xi} + \beta \xi \tag{12}$$

where $\Xi : \mathbb{R} \to \mathcal{Q}$ represents a subsequently defined customizable, continuously differentiable, admitted position trajectory generated using the admittance filter in (10) [i.e., $\Xi = f(q_a)$], $\beta \in \mathbb{R}_{>0}$ denotes a constant control gain, and ψ acts as a second sliding surface. Although the admitted trajectory is generated online, it determines if pedals of the cycle act as if they are coupled or decoupled. That is, if both sides share the same admitted trajectory, symmetry is preserved, the pedals will appear to be coupled, and the two sides of the cycle will operate at the same cadence. Otherwise, each side will have a unique admitted trajectory, symmetry will be broken, the pedals will be decoupled, and the two sides will operate at their own independent cadence. The motivation behind such a design is to establish a framework, for which numerous trajectories can be investigated to best promote rehabilitation outcomes without modifying the developed controller. The open-loop admittance error system is generated by taking the time derivative of (12), multiplying by M, adding and subtracting ξ, and substituting (1), (11), and (12) to yield

$$M\dot{\psi} = Y\theta + \Upsilon - \tau_m - B_e u_e - \xi - V\psi \tag{13}$$
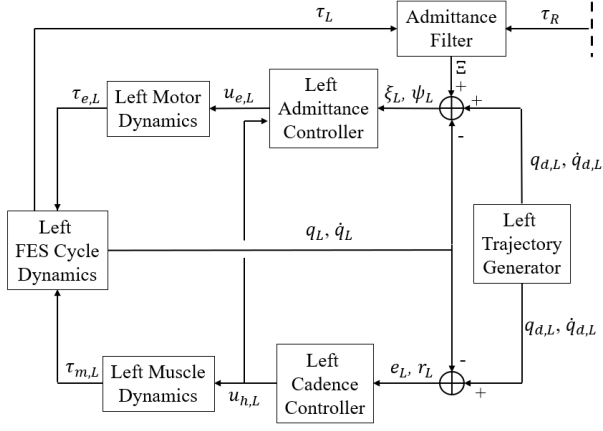
Fig. 1. Block diagram showing the cadence and admittance controllers on the left side of the split-crank FES cycle. The subscripts L and R are used to denote signals on the left and right sides of the FES cycle. Note, the admittance trajectory denoted by Ξ is a function of the admitted trajectory, q_a, which is a function of both the torque on the left and right sides of the split-crank cycle.

$$
\begin{aligned}
Y\theta \triangleq\ & M(\ddot{\Xi} + \ddot{q}_d + \beta\psi - \beta^2\xi) \\
& + V(\dot{\Xi} + \dot{q}_d + \beta\xi) + G \\
& + b(\dot{\Xi} + \dot{q}_d - \psi + \beta\xi)
\end{aligned} \tag{14}
$$

where $Y : \mathbb{R}^2 \times \mathbb{R}_{\geq 0} \to \mathbb{R}^{1 \times 8}$ denotes a computable regression matrix and by Property 2 is linear in the parameters; and $\theta \in \mathbb{R}^{8 \times 1}$ denotes a matrix of constant system parameters. The lumped auxiliary signal $\Upsilon : \mathcal{Q} \times \mathbb{R} \times \mathbb{R}_{\geq 0} \to \mathbb{R}$ is defined as $\Upsilon \triangleq P + d + \xi$ and is bounded by Property 1 as $|\Upsilon| \leq c_4 + c_5\|\phi\|$, where $c_4,\ c_5 \in \mathbb{R}_{>0}$ are known constants, and the error vectors $\phi \in \mathbb{R}^3$ and $\zeta \in \mathbb{R}^2$ are defined as $\phi \triangleq [\zeta^T, \ \dot{\Xi}]^T$ and $\zeta \triangleq [\xi, \ \psi]^T$, respectively. Based on (13) and the subsequent stability analysis, the admittance controller is designed as

$$
u_e \triangleq \frac{1}{B_e}(Y\hat{\theta} + k_5\psi + (k_6 + k_7\|\phi\| + k_8|u_h|)\operatorname{sgn}(\psi)) \tag{15}
$$

where $k_i \in \mathbb{R}_{>0}\ \forall i \in \{5,\ 6,\ 7,\ 8\}$ denote constant control gains, and $\hat{\theta} : \mathbb{R}_{\geq 0} \to \mathbb{R}^{8 \times 1}$ denotes a time-varying estimate of the constant system parameters. Based on the subsequent stability analysis, the estimates for the system parameters in (14) are generated online according to

$$
\dot{\hat{\theta}} \triangleq \operatorname{proj}(\Gamma Y^T \psi) \tag{16}
$$

where $\Gamma \in \mathbb{R}^{8 \times 8}$ denotes a constant positive definite learning gain, and $\operatorname{proj}(\cdot)$ denotes a projection algorithm operator [51, Sec. 4.4]. Substituting (15) into (13) yields the closed-loop admittance error system

$$
\begin{aligned}
M\dot{\psi} =\ & \Upsilon - \tau_m - V\psi - \xi + Y\tilde{\theta} - k_5\psi \\
& - (k_6 + k_7\|\phi\| + k_8|u_h|)\operatorname{sgn}(\psi)
\end{aligned} \tag{17}
$$

where $\tilde{\theta} : \mathbb{R}_{\geq 0} \to \mathbb{R}^{8 \times 1}$ denotes the error between the actual and estimated system parameters. A block diagram of the dual-controller structure is shown in Fig. 1.

IV. STABILITY ANALYSIS

To facilitate the following theorems, let $W_L : \mathbb{R}^2 \to \mathbb{R}$ denote a continuously differentiable, positive definite storage function defined as

$$
W_L \triangleq \frac{1}{2}Mr^2 + \frac{1}{2}e^2 \tag{18}
$$

and let $V_L : \mathbb{R}^{10} \to \mathbb{R}$ denote a continuously differentiable, positive definite Lyapunov function candidate defined as

$$
V_L \triangleq \frac{1}{2}M\psi^2 + \frac{1}{2}\xi^2 + \frac{1}{2}\tilde{\theta}^T \Gamma^{-1}\tilde{\theta}. \tag{19}
$$

Theorem 1: The closed-loop cadence error system in (9) is passive from input $|\tau_e + \chi|$ (i.e., the motor torque and system disturbances) to output $|r|$, with the storage function W_L, $\forall t$.

Proof: Let $z : \mathbb{R}_{\geq 0} \to \mathbb{R}^2$ for $t \in [t_0, \infty)$ be a Filippov solution to the differential inclusion $\dot{z} \in K[h](z)$, where $K[\cdot]$ is defined as in [52], and $h : \mathbb{R}^2 \to \mathbb{R}^2$ is defined as $h \triangleq [\dot{e}, \ \dot{r}]^T$. Because of the discontinuity in the muscle controller in (8), the time derivative of W_L exists almost everywhere (a.e.) [i.e., for almost all $t \in [t_0, \infty)$], and $\dot{W}_L(z) \overset{\text{a.e.}}{\in} \dot{\tilde{W}}_L(z)$, where $\dot{\tilde{W}}_L$ is the generalized time derivative of W_L along the Filippov trajectories of $\dot{z} = h(z)$ [53]. Using the calculus of $K[\cdot]$ from [53], and substituting (6) and (9) into $\dot{\tilde{W}}_L$ yields

$$
\begin{aligned}
\dot{\tilde{W}}_L \subseteq\ & -\alpha e^2 + r\chi + \left(\frac{1}{2}\dot{M} - V\right)r^2 \\
& - \sum_{m \in \mathcal{M}} K[B_m\sigma_m]\operatorname{sat}_\rho\Bigg[\frac{1}{B_{\underline{m}}}(k_1 r^2 + (k_2 + k_3\|z\| \\
& \hspace{3cm} + k_4\|z\|^2)K[\operatorname{sgn}(r)]r)\Bigg] - r\tau_e
\end{aligned} \tag{20}
$$

where $K[B_m\sigma_m] \triangleq \{0,\ B_m\}$. For $q \in \mathcal{Q}_M$, $\sum_{m \in \mathcal{M}} K[B_m\sigma_m]$ is nonzero and may be bounded by Property 4 as $B_{\underline{m}}$, which is continuous. In the case where the control input is below saturation (i.e., $u_h \leq \rho$), by Properties 1 and 3, and since $\dot{W}_L(z) \overset{\text{a.e.}}{\in} \dot{\tilde{W}}_L(z)$, (20) can be bounded as

$$
\begin{aligned}
\dot{W}_L \overset{\text{a.e.}}{\leq}\ & -\alpha e^2 - k_1 r^2 - \lambda_1|r| - \lambda_2|r|\|z\| \\
& - \lambda_3|r|\|z\|^2 + |r||\tau_e|
\end{aligned} \tag{21}
$$

where $\lambda_1,\ \lambda_2,\ \lambda_3 \in \mathbb{R}$ are defined as $\lambda_1 \triangleq k_2 - c_1$, $\lambda_2 \triangleq k_3 - c_2$, and $\lambda_3 \triangleq k_4 - c_3$ and where $c_1,\ c_2,$ and c_3 are the bounding constants on χ in (7). Provided $k_2 \geq c_1$, $k_3 \geq c_2$, $k_4 \geq c_3$, then $\lambda_1,\ \lambda_2,\ \lambda_3 \geq 0$; thus, (21) can be bounded further as

$$
\dot{W}_L \overset{\text{a.e.}}{\leq} -\alpha e^2 - k_1 r^2 + |r||\tau_e|. \tag{22}
$$

Because the interaction torque is bounded, the physically applied motor torque is similarly bounded [10], [17]. Hence, by [50, Definition 6.3] the cadence error system is output strictly passive with input $|\tau_e|$, output $|r|$, and storage function W_L, and the cadence controller is bounded (i.e., $u_h \in \mathcal{L}_\infty$). Using similar arguments for the case where the control input is saturated (i.e., $u_h > \rho$), (20) can be bounded as

$$
\dot{W}_L \overset{\text{a.e.}}{\leq} |r||\tau_e + \chi|. \tag{23}
$$

Because the admittance and position error systems are coupled (i.e., $\zeta = \Xi + e$) and because the admittance trajectory is bounded (i.e., q_a, $\dot{q}_a$ $\ddot{q}_a \in \mathcal{L}_\infty$), if $|\xi|$ and $|\psi|$ are bounded, then $|e|$ and $|r|$ are likewise bounded. By the definition of χ in (7) and Property 1, if $|e|$ and $|r|$ are bounded, then $|\chi|$ is bounded. Hence, by [50, Definition 6.3] the cadence error system can be shown to be passive with the input $|\tau_e + \chi|$, output $|r|$, and storage function W_L, as long as $|\xi|$ and $|\psi|$ are bounded, which is the direct result of the subsequent theorem. It can also be shown that (22) can be bounded with (23) which provides the result of Theorem 1. ∎

Remark 1: Although the above-mentioned analysis does not include volitional contribution from the rider, a common assumption in human–robot interaction is that the human is naturally passive [22]. If the rider volitionally contributes, the cadence controller and rider would act in parallel. Because passive systems in parallel remain passive [50], volitional contributions would not affect $|r|$ being passive with respect to the motor torque and system disturbances (i.e., $|\tau_e + \chi|$). Hence, the rider is able to volitionally contribute toward the tracking objective without destabilizing the cadence error system.

Theorem 2: Given the closed-loop error system in (17), the admittance controller globally asymptotically regulates the admittance error system in the sense that $\zeta \triangleq [\,\xi,\ \psi\,]^T \to 0$ as $t \to \infty$, provided the following constant gain conditions are satisfied: $k_6 \geq c_4$, $k_7 \geq c_5$, $k_8 \geq B_{\overline{m}}$, where c_4 and c_5 are the bounding constants on Υ in (13), and $B_{\overline{m}}$ was introduced in Property 4.

Proof: Using an argument similar to the proof for Theorem 1, the time derivative of (19) can be bounded above using (12), (17), and Properties 1, 3, and 4 as

$$\dot{V}_L \overset{\text{a.e.}}{\leq} -\beta\xi^2 - k_5\psi^2 - |\psi|(\lambda_4 + \lambda_5\|\phi\| + \lambda_6|u_h|) \quad (24)$$

where λ_4, λ_5, $\lambda_6 \in \mathbb{R}$ are defined as $\lambda_4 \triangleq k_6 - c_4$, $\lambda_5 \triangleq k_7 - c_5$, and $\lambda_6 \triangleq k_8 - B_{\overline{m}}$. Provided the gain conditions listed in Theorem 2 are satisfied, λ_4, λ_5, $\lambda_6 \geq 0$, and thus, (24) can be upper bounded as

$$\dot{V}_L \overset{\text{a.e.}}{\leq} -\beta\xi^2 - k_5\psi^2. \quad (25)$$

Hence, (19) is a common Lyapunov function across both the FES and KDZ regions. Subsequently, [54] can be invoked, along with the radially unboundedness of (19), to show $|\xi|$, $|\psi|$, $\|\zeta\| \to 0$ as $t \to \infty$. Since $V_L > 0$ and $\dot{V}_L \overset{\text{a.e.}}{\leq} 0$, $V_L \in \mathcal{L}_\infty$, and hence, ξ, ψ, $\tilde{\theta} \in \mathcal{L}_\infty$, which implies $\dot{q}$, $\hat{\theta} \in \mathcal{L}_\infty$. Since (10) is passive, $\dot{q}_a$, $\ddot{q}_a \in \mathcal{L}_\infty$, which implies Y, $\|\phi\| \in \mathcal{L}_\infty$. Finally, because $u_h \in \mathcal{L}_\infty$, $u_e \in \mathcal{L}_\infty$. ∎

V. EXPERIMENTS

A. Testbed

The experiments were conducted on a motorized split-crank FES cycle, which is a modified version of the testbed described in [27], except with encoders and motors on both sides of the cycle, mounted in a mirrored configuration, as shown in Fig. 2. The motors are controlled with an ADVANCED
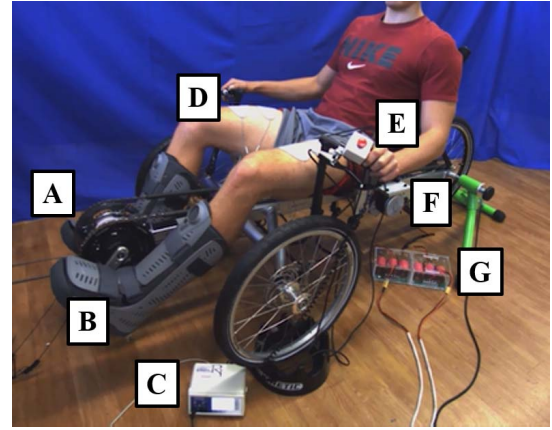

Fig. 2.   Motorized split-crank FES cycle with: A. Right encoder and powermeter. B. Left encoder and powermeter. C. Stimulator. D. Electrodes (quadriceps shown). E. Emergency stop. F. Right and left motors (left shown). G. Filter cards.

Motion Controls[5] (AMC) PS300W24 power supply, an AMC AB25A100 motor driver, and an AMC FC15030 filter card. SRM science road wireless power meters are mounted to each side of the bike crank to measure the interaction torque between the right and left side of the rider and the cycle. A Hasomed Rehastim 1 current-controlled stimulator delivered biphasic, symmetric, rectangular pulses to the participant's muscle groups via bipolar, self-adhesive, PALS electrodes.[6] The stimulation was applied at 60 Hz, and amplitudes were fixed at 90, 80, and 70 mA for the quadriceps, hamstrings, and gluteals, respectively. The stimulation pulsewidth for each muscle group was determined by the controller in (8) and commanded to the stimulator by the control software. An emergency stop button was fastened to the tricycle that enabled the participant to immediately stop the experiment if desired.

B. Methods

Experiments were conducted on one able-bodied male participant, aged 26-years old (P1), one male participant with spina bifida, aged 25-years old (P2), one female participant with poststroke right-sided hemiparesis, aged 50-years old (P3), and one male participant with Parkinson's disease, aged 64-years old (P4). P2 has spina bifida (L5-S1) with an Arnold Chiari malformation and regularly participates in physical therapy; he uses ankle-foot orthoses and a wheelchair and is familiar with FES. P3 had a stroke in 2014 and is community ambulatory without aid; she has regained some function in her right leg (her affected leg) though this was her first experience with FES cycling. P4 was diagnosed with Parkinson's disease in 1997 and regularly participates in physical therapy and exercise; although he had a noticeable tremor in both arms, his right arm had a larger magnitude. A single trial of two primary protocols was conducted on each participant, Protocol A, which implemented the controllers in (8) and (15),

---

[5]AMC supported the development of this testbed by providing discounts on their branded items.

[6]Surface electrodes for this study were provided compliments of Axelgaard Manufacturing Company Ltd., Fallbrook, CA, USA.

and Protocol B, which also implemented the controllers in (8) and (15), but with the adaptive feedforward component disabled (i.e., $\Gamma = 0$). Participants 1–4 completed both Protocols A and B in random order, with P1 receiving stimulation only on the quadriceps muscle group for proof of concept, and P2–P4 receiving stimulation on the quadriceps, hamstrings, and gluteal muscle groups. For Protocols A and B, the participants were asked not to contribute volitionally; although some volitional contribution is possible and not measured, any voluntary contribution was only partially informed by stimulation cues because participants were unaware of the desired trajectories. To investigate the effect of adding volition, P4 was asked to repeat Protocol A with volition, denoted by Protocol C. During this protocol, P4 was only shown a plot of the desired cadence and the measured cadence for their right side.

While there is no clear consensus for the optimal cadence of FES cycles for rehabilitation, it has been suggested that lower cadences may be more ideal for torque production, while higher cadences may be better for power production [46]. However, for feasibility purposes, the desired cadence was set to 50 RPM [55], [56] for both the able-bodied population and the population with NCs, without loss of generality. Each protocol had a total duration of 180 s, with the first 20 s consisting of a smooth motor-only ramp to the desired cadence. After the initial ramp, the controllers in (8) and (15) were switched on and errors were recorded. For all protocols except Protocol C, the participants were blind to the desired trajectories for the duration of the experiment. The experimental protocols were approved by the Institutional Review Board at the University of Florida, Gainesville, FL, USA (IRB201600881). For all experiments, the admittance parameters in (10) were selected as $B_d = 1$ (Nm · s/rad), $M_d = 2$ (Nm · s^2/rad), $\tau_d = 0.5$ Nm for P1, $\tau_d = 0.2$ Nm for P2, $\tau_d = 0.3$ Nm for P3, and $\tau_d = 0.2$ Nm for P4. The controller gains in (6), (8), (12), (15), and (16) were selected as $k_1 \in [3.0, 5.5]$, $k_2 = k_3 = k_4 = 0.1$, $k_5 \in [5.0, 10.0]$, $k_6 = k_7 = k_8 = k_9 = 0.001$, $\alpha \in [2.0, 3.5]$, $\beta \in [0.1, 0.2]$, and $\Gamma = 0.1 \cdot \text{diag}(3.15, 3.15, 1.05, 2.10, 5.25, 5.25, 1.05, 0.63)$.

To account for the electromechanical delay present in the rider's muscles, the stimulation pattern was advanced as a function of the cadence (i.e., $q_{\text{stim}} \triangleq q + 0.1\dot{q}$), where $q_{\text{stim}} : \mathcal{Q} \times \mathbb{R} \to \mathcal{Q}$ was substituted for q in (4). Although the aforementioned gain conditions are sufficient to achieve stability for the largest uncertainties on the system parameters, they represent conservative gains required by the controllers in (8) and (15). Therefore, the gain conditions provide guidelines for the initial gain selection, and the gains can be subsequently adjusted to achieve the desired performance. The listed gains were adjusted using an empirical-based method, but the gains could have been adjusted using more methodical approaches. For example, the nonlinear system in [57] was linearized at several operating points, and a linear controller was designed for each point, and the gains were chosen by interpolating or scheduling the linear controllers. In [58], a neural network is used to tune the gains of a proportional, integral, derivative (PID) controller. In [59], a genetic algorithm was used to fine-tune the gains after initialization, and guesses

were made by the controller designer. Killingsworth and Krstic [60] provide an extensive discussion on the use of extremum seeking for tuning the gains of a PID controller. In addition, in [61], the tuning of a PID controller for robot manipulators is discussed.

The admitted trajectory in the error system in (11) and (12) was generated using $\Xi \triangleq (1/2)(q_{a,L} + q_{a,R})$, where $q_{a,x} : \mathbb{R}_{\geq 0} \to \mathbb{R}$, $\forall x \in \mathcal{X} \triangleq \{L, R\}$ represent the trajectories generated using the admittance filter in (10) for the left and right sides of the cycle, respectively. The motivation behind the admitted trajectory being an average of the two sides is to synchronize the positions and cadences of each side, so the natural coordination and symmetry of the legs are preserved. This trajectory strikes a dynamic balance between the capabilities of both legs instead of holding the legs to a standard which they may be incapable of reaching (e.g., having a nondominant leg track the trajectory generated from a dominant leg); instead, the trajectory is set to the average capabilities of the legs, such that the more capable leg experiences resistance and the less capable leg experience assistance. However, many different trajectories could be selected, with potential clinical differences. For example, the results in [46] suggests that lower cadences may be optimal for strength training, but higher cadences may be best for power training.

C. Results

Let participants and protocols be referred to by their respective numbers and letter; for example, Participant 1 running Protocol B is referred to as P1B. Numerical results for Protocols A and B are displayed in Table I with details on the average and standard deviation of the measured cadence, admitted cadence, admitted cadence tracking error, motor control input, and measured torque for each leg. As shown in Table I, the average cadences for each leg (i.e., $\dot{q}_x$, $\forall x \in \mathcal{X}$) were similar with adaptation enabled and disabled. However, with adaptation, the standard deviation of the admitted tracking error was reduced by 75% for P1, 19% for P2, 47% for P3, and 50% for P4. Compared with our most similar previous result on single-crank FES cycling, which utilized robust admittance control (i.e., [32]), the robust version of the presented controller (i.e., Protocol B) demonstrated a notably higher standard deviation of $\dot{\xi}$ for the same participant, Participant A (i.e., -0.10 ± 1.87 RPM in [32] compared with -0.13 ± 5.33 RPM on the left side of the split-crank cycle). It is surmised that this difference is largely due to the split-crank cycle's susceptibility to gravitational effects (i.e., they are not canceled as in single-crank cycling). By subsequently enabling adaptation on the split-crank cycle to compensate for dynamics (e.g., inertial, centripetal-Coriolis, gravitational, and friction effects), the admittance cadence error presented here then more closely resembles our previous work (i.e., -0.10 ± 1.87 RPM in [32] compared with -0.23 ± 1.64 RPM).

Graphical results for P1–P4 running Protocol A are provided in Figs. 3–10. Figs. 3, 5, 7, and 9 show the cadence tracking results along with the root-mean-square (rms) (windowed at 0.5 s) values of $\dot{\xi}$ and $\dot{e}$ for P1A, P2A, P3A, and P4A, respectively. Figs. 4, 6, 8, and 10 show the control inputs to

TABLE I

EXPERIMENTAL RESULTS, REPORTED AS AVERAGE ± STANDARD DEVIATION

Participant	Protocol	$\dot{q}_L$ (RPM)*	$\dot{q}_R$ (RPM)*	$\dot{q}_\alpha$ (RPM)†	$\dot{\xi}_L$ (RPM)	$\dot{\xi}_R$ (RPM)	$u_{e,L}$ (A)	$u_{e,R}$ (A)	τ_L (Nm)	τ_R (Nm)
1	A	49.03±1.73	48.92±1.16	48.80±0.84	-0.23±1.64	-0.13±0.94	-2.42±4.64	1.98±4.69	0.20±3.70	0.15±3.51
	B	47.70±4.90	47.63±5.18	47.58±0.91	-0.13±5.33	-0.05±4.67	-2.59±4.89	2.55±5.35	0.00±3.68	-0.27±3.60
2	A	49.00±1.60	48.98±1.52	48.89±0.09	-0.11±1.60	-0.10±1.53	-2.32±2.73	2.09±2.97	-0.13±1.54	-0.05±1.60
	B	48.63±2.06	48.58±1.78	48.60±0.39	-0.03±1.87	0.30±1.97	-2.38±2.13	2.15±2.63	-0.19±1.55	-0.08±1.55
3	A	48.87±1.40	48.82±1.31	48.74±0.27	-0.13±1.40	-0.09±1.26	-1.97±2.94	2.20±3.01	0.22±2.33	-0.09±2.20
	B	48.50±2.75	48.46±2.43	48.43±0.37	-0.08±2.73	-0.03±2.39	-1.99±3.12	2.37±3.25	0.17±2.33	-0.20±1.95
4	A	49.91±1.46	49.81±2.41	49.72±0.84	-0.19±1.52	-0.09±2.16	-1.91±3.77	2.35±5.15	0.17±2.56	0.07±4.04
	B	49.65±3.68	49.53±4.02	49.51±0.86	-0.14±3.65	-0.03±3.81	-2.21±4.08	2.59±5.03	-0.03±2.49	-0.17±4.10
	C	50.26±1.73	50.16±2.70	49.94±0.83	-0.20±1.87	-0.10±2.40	-1.46±4.11	2.10±5.43	0.36±2.70	0.66±4.37
Mean‡	A	49.20±1.79	49.13±1.93	49.03±0.70	-0.16±1.78	-0.10±1.77	-2.15±4.15	2.15±4.70	0.11±3.05	0.02±3.46
	B	48.62±4.05	48.55±4.16	48.53±0.78	-0.09±4.19	0.04±3.91	-2.29±4.27	2.41±4.87	-0.01±3.03	-0.18±3.46

*At steady state, the average cadence error is given as $\dot{e}_x = 50 - \dot{q}_x, \; \forall x \in \mathcal{X}$.
†$\dot{q}_\alpha : \mathbb{R}_{\geq 0} \to \mathbb{R}$ denotes the average admitted cadence given as $\dot{q}_\alpha \triangleq \dot{q}_d + \frac{1}{2}\left(\dot{q}_{a,L} + \dot{q}_{a,R}\right)$, identical for both legs.
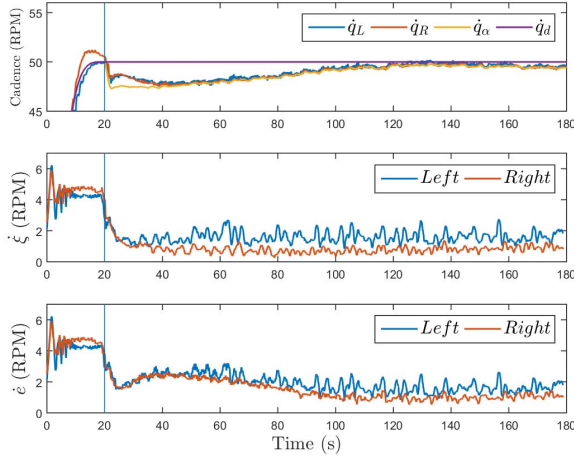‡Protocol C was not included in calculating the mean.

Fig. 3. P1A (Top) The measured cadence for the left ($\dot{q}_L$) and right ($\dot{q}_R$) leg, admitted cadence ($\dot{q}_a$), and desired cadence ($\dot{q}_d$); (Middle) rms error of $\dot{\xi}$ for the left and right legs; and (Bottom) rms error of $\dot{e}$ for the left and right legs. Vertical lines represent the time of controller activation.
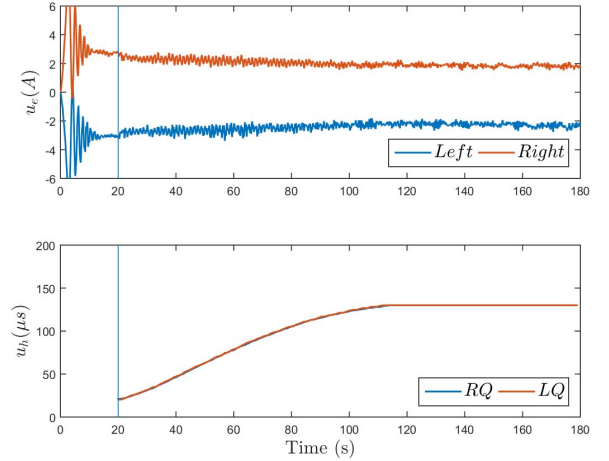

Fig. 4. P1A (Top) Control inputs to left and right motors and (Bottom) control inputs to the rider's quadriceps femoris muscle groups for the left and right legs. Because the motors are mounted in a mirrored configuration, they require opposite signs on the delivered current. The muscle gains for the left and right quadriceps were identical, and therefore, the stimulation closely overlaps. The stimulation input was saturated at 130 μs for rider comfort.

the cycle's motors and rider's muscle groups for P1A, P2A, P3A, and P4A, respectively. For visual clarity, a half-second moving average filter was applied to all plots displaying measured cadences and motor control inputs (i.e., $\dot{q}_L$, $\dot{q}_R$, and u_e). To directly compare results with and without adaptation, Figs. 11 and 12 are included for P4B, which display the cadence tracking results and control inputs, respectively. To examine the effects of the rider volitionally pedaling alongside the admittance and cadence controllers, Figs. 13 and 14 display P4C, which is P4 running Protocol A with added volition.

D. Discussion

Across all participants, adding adaptation to the admittance controller resulted in improvement in the cadence tracking performance in terms of the average cadence error and standard deviation. A reduction in the standard deviation of the cycle's cadence is a result of more uniform cadence tracking, which results in smoother cycling performance. Consequently, this reduces the variation of the cadence errors and assists in

smoothing out the applied stimulation to the rider's muscles, resulting in a more comfortable experience for the rider. By examining the results of P1, the effects of adaptation are evident; in Fig. 3, the rms value of $\dot{\xi}$ decreases steadily for the first 20 s after controller activation. In addition, as the stimulation input increases, the rider produces more torque and is able to contribute more toward the cadence tracking objective (compare Figs. 3 and 4). Furthermore, as the admittance controller adapts, and the rider generates more torque, the control effort required by the motors is reduced throughout the experiment, as shown in Fig. 4. Based on Table I, adaptation improved all metrics except for a slight increase in $\dot{\xi}$ (i.e., from -0.13 RPM to -0.23 RPM for the left side, and from -0.05 RPM to -0.13 RPM for the right side). In fact, with adaptation, the standard deviation of the measured cadence was reduced by 65% and 78% for the left and right sides, respectively, and the standard deviation of the admitted cadence was reduced by 69% and 80% for the left and right sides, respectively.
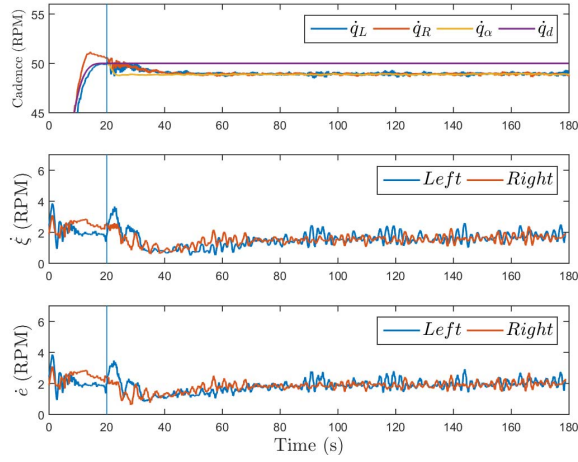
Fig. 5. P2A (Top) the measured cadence for the left ($\dot{q}_L$) and right ($\dot{q}_R$) leg, admitted cadence ($\dot{q}_a$), and desired cadence ($\dot{q}_d$); (Middle) rms error of $\dot{\xi}$ for the left and right legs; and (Bottom) rms error of $\dot{e}$ for the left and right legs.

Fig. 7. P3A (Top) the measured cadence for the left ($\dot{q}_L$) and right ($\dot{q}_R$) leg, admitted cadence ($\dot{q}_a$), and desired cadence ($\dot{q}_d$); (Middle) rms error of $\dot{\xi}$ for the left and right legs; and (Bottom) rms error of $\dot{e}$ for the left and right legs.
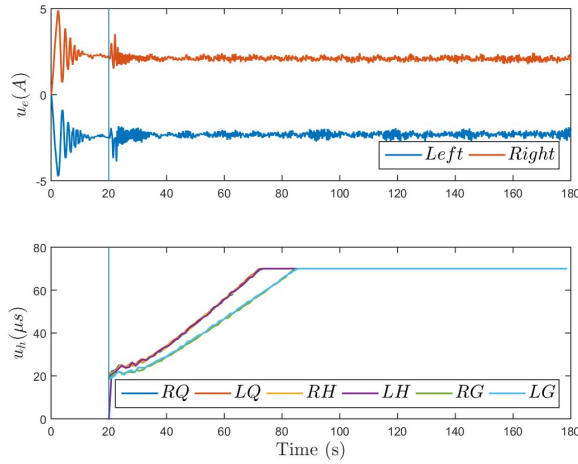

Fig. 6. P2A (Top) control inputs to left and right motors and (Bottom) control inputs to the rider's right (R) and left (L) quadriceps (Q), hamstring (H), and gluteal (G) muscle groups. The stimulation input was saturated at 65 μs for rider comfort.

Fig. 8. P3A (Top) control inputs to left and right motors and (Bottom) control inputs to the rider's right (R) and left (L) quadriceps (Q), hamstring (H), and gluteal (G) muscle groups. The stimulation input was saturated at 40 μs for the right hamstring and gluteal and 45 μs for all other muscle groups.

When comparing P2 with P1, it is noted P2 had a lower stimulation limit and experienced fatigue at a quicker rate, despite all muscle groups being stimulated. The low stimulation limit made the experiments of P2A and P2B appear very similar in nature (i.e., with and without adaptation), except the adaptation resulted in smoother cadence tracking/performance. Due to adaptation of the motor controller, it can be seen in Fig. 5 that the rms value of $\dot{\xi}$ was reduced over the course of the experiment, despite only a subtle reduction in the motor control effort, as shown in Fig. 6. According to Table I, the adaptation was able to reduce the standard deviation of the measured cadence by 32% and 15% for the left and right sides, respectively, and of the admitted cadence by 14% and 32% for the left and right sides, respectively. Because P2's stimulation was saturated early in the experiment, he was unable to achieve the desired cadence at the desired interaction torque. However, because the admittance controller held the admitted cadence trajectory near the desired cadence trajectory, the robot-assisted the rider in maintaining
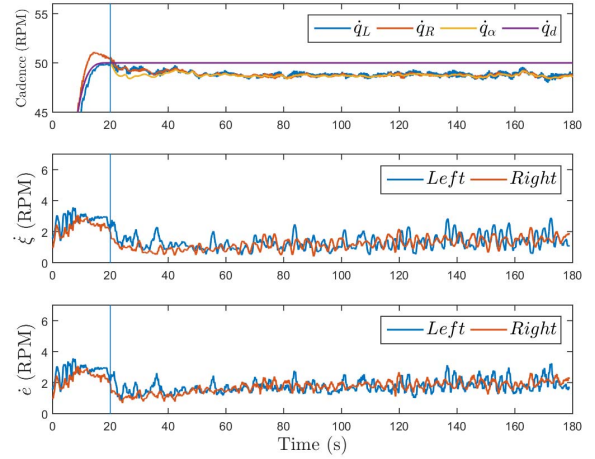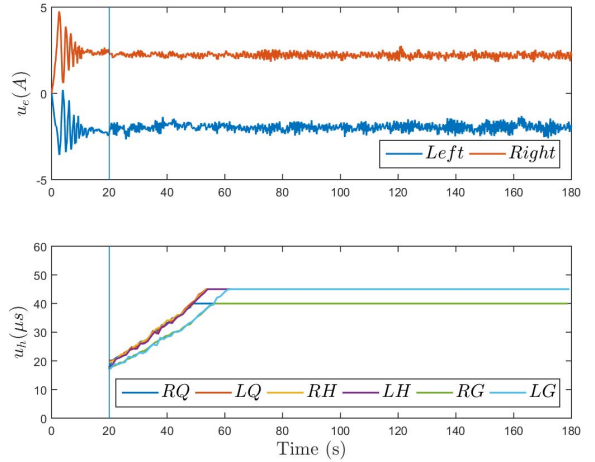
his cadence. This exemplifies the assist-as-needed control paradigm because, without the admittance controller, the rider would have been unable to produce an identical cadence. Because the cadence controller is passive and the admittance controller demonstrates asymptotic tracking, the FES cycle exemplifies stable performance through the remaining portion of the experiment. Although P2 has spina bifida, the cycle detected no notable asymmetries in performance; this was reasonable considering P2 uses ankle-foot orthoses on both legs and symmetric walking aids (i.e., walkers and wheelchairs).

Because P3 had previously had a stroke which compromised her right leg, it was anticipated that P3 would showcase the cycle's ability to address asymmetries. However, P3 presented a strong sensitivity (i.e., hypersensitivity) to stimulation, and thus, the amount of stimulation that could be applied (and hence, torque contribution) was minimal. Similar to P2, P3's stimulation was saturated early in the experiment; however,
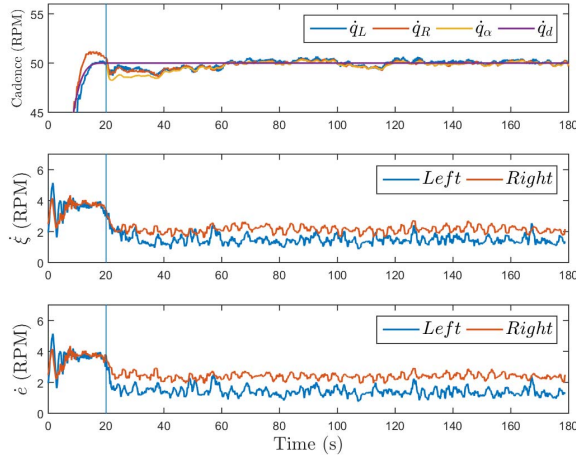
Fig. 9. P4A (Top) the measured cadence for the left ($\dot{q}_L$) and right ($\dot{q}_R$) leg, admitted cadence ($\dot{q}_a$), and desired cadence ($\dot{q}_d$); (Middle) rms error of $\dot{\xi}$ for the left and right legs; and (Bottom) rms error of $\dot{e}$ for the left and right legs.

Fig. 11. P4B (Top) the measured cadence for the left ($\dot{q}_L$) and right ($\dot{q}_R$) leg, admitted cadence ($\dot{q}_a$), and desired cadence ($\dot{q}_d$); (Middle) rms error of $\dot{\xi}$ for the left and right legs; and (Bottom) rms error of $\dot{e}$ for the left and right legs.
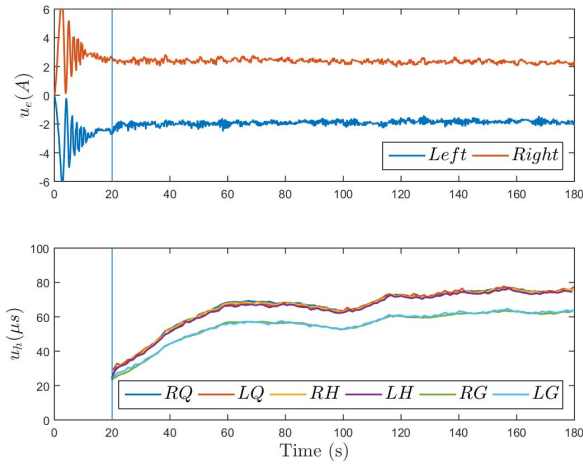

Fig. 10. P4A (Top) control inputs to left and right motors and (Bottom) control inputs to the rider's right (R) and left (L) quadriceps (Q), hamstring (H), and gluteal (G) muscle groups.

Fig. 12. P4B (Top) control inputs to left and right motors and (Bottom) control inputs to the rider's right (R) and left (L) quadriceps (Q), hamstring (H), and gluteal (G) muscle groups.

unlike P2, P3's saturation limit was much lower (i.e., 65 μs for P2 compared with 40–45 μs for P3). Despite the lower saturation levels, the cycle was still able to adapt and asymptotically track the admittance error system. According to Table I, her unimpaired leg (left) generated more torque than her impaired leg (right), and both legs demonstrated improved tracking performance with adaptation enabled. With adaptation, the standard deviation of the measured cadence was reduced by 49% and 46% for the left and right sides, respectively, and the standard deviation of the admitted cadence was reduced by 49% and 47% for the left and right sides, respectively. Fig. 7 shows cadence tracking performance and Fig. 8 shows the control efforts for P3A. From a rehabilitation perspective, it would be beneficial for P3 to acclimate to the sensation of neuromuscular electrical stimulation before participating in additional FES cycling exercises; as stated, this experiment was her first experience with electrical stimulation. After some acclimation, it is assumed she would be able to tolerate a higher stimulation limit, which would allow
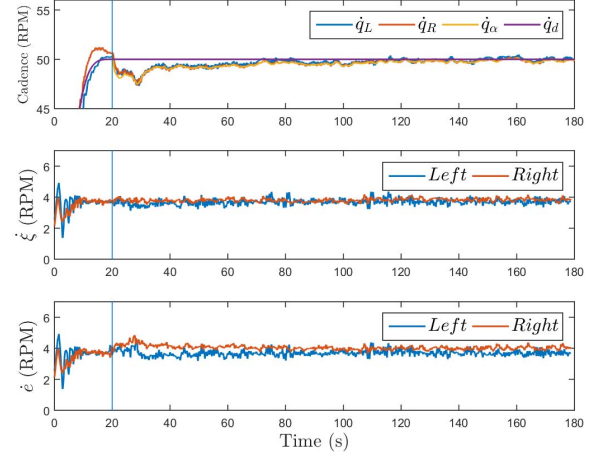
for stronger muscle contractions and better measurement of muscular asymmetries.

To directly examine the effects of adding adaptation to the admittance controller, Figs. 9 and 10 display the tracking results and control inputs with adaptation enabled for P4 and Figs. 11 and 12 display the tracking results and control inputs with adaptation disabled for P4. By directly comparing Figs. 9–11, it can be seen that immediately after controller activation, the rms admittance and cadence tracking errors decayed to nearly half their pre-activation values when adaptation was activated. Although the adaptation only occurs on the robot, because the robot and the rider are physically coupled, improved performance from the admittance controller yielded improved performance from the cadence controller. This effect is significant because of the challenges when adding adaptation to the cadence controller due to the unknown, nonlinear muscle control effectiveness in (2); hence, adaptation can be added to the robot's controller to improve performance of the cadence

Fig. 13. P4C (Top) the measured cadence for the left ($\dot{q}_L$) and right ($\dot{q}_R$) leg, admitted cadence ($\dot{q}_a$), and desired cadence ($\dot{q}_d$); (Middle) rms error of $\dot{\xi}$ for the left and right legs; and (Bottom) rms error of $\dot{e}$ for the left and right legs.
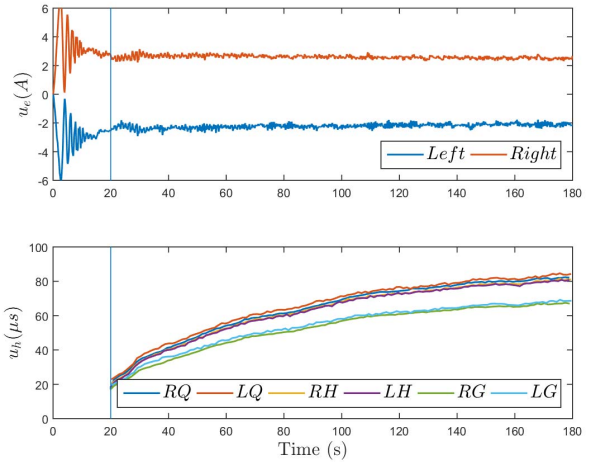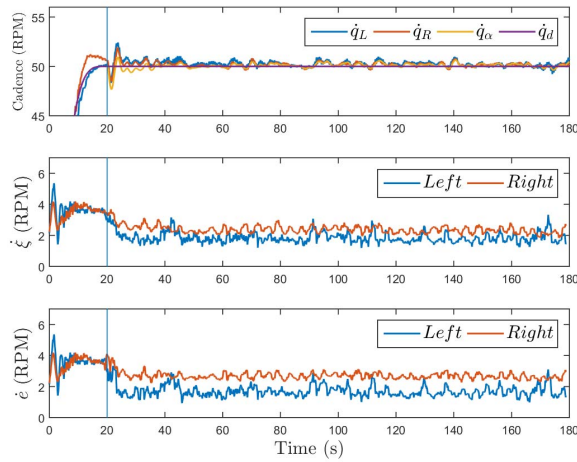

Fig. 14. P4C (Top) control inputs to left and right motors and (Bottom) control inputs to the rider's right (R) and left (L) quadriceps (Q), hamstring (H), and gluteal (G) muscle groups.

controller applied to the rider's muscles. As with all other participants, the adaptive controller was able to reduce the standard deviation of the measured cadence (by 60% and 40% for the left and right sides, respectively) and the admitted cadence (by 58% and 43% for the left and right sides, respectively). This resulted in smoother cycling performance and more uniform stimulation patterns, which is desirable to promote rider comfort. P4 did not reach his stimulation limit in either protocol (see Figs. 10 and 12) and, as shown in Figs. 9 and 11, was able to produce enough interaction torque to align the admitted cadence trajectory with the desired cadence trajectory.

To compare the effect of adding rider volition alongside the admittance and cadence controllers, Protocol C was run on P4. As shown in Fig. 13, the tracking errors demonstrated similar convergence to P4A, the protocol without volition or adaptation. As displayed by Table I, in this instance, the controllers outperformed at tracking the desired trajectories than the rider was able to with volition while monitoring his performance. In contrast, the rider was able to generate a larger interaction torque when volition was included. Because the rider was able to track the desired cadence trajectory accurately and quickly (i.e., the stimulation did not require error accumulation to ramp up), the rider's stimulation was kept well below his saturation threshold to the point where he was unable to perceive it. According to Table I, P4 surpassed the desired interaction torque, the cycle's average cadence was above the desired, the cycle resisted the rider, and the rider's stimulation was withdrawn (see Fig. 14).

Regardless of the controller, Figs. 3, 5, 7, and 9 indicate that the measured cadences fluctuate around the desired value throughout the experiment. The cause of these fluctuations can arise from system disturbances, such as chain links, the rider, or inaccurate modeling. Because each controller is designed to account for these disturbances, when the disturbance occurs, the controller is capable of compensating for it and correcting the measured trajectory. The degree of these fluctuations can be quantified using the standard deviation of cadence,
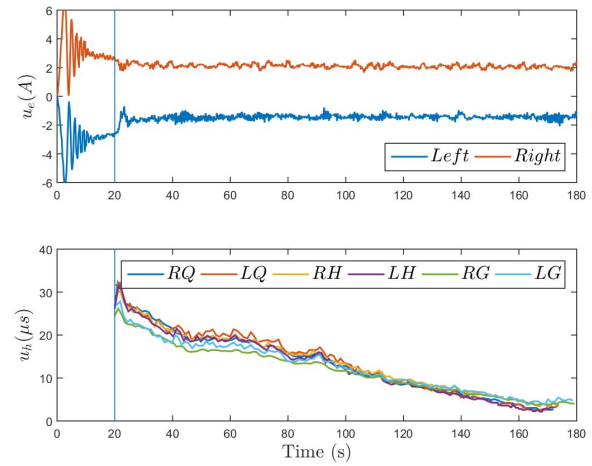
displayed in Table I. Across all trials, the participants begin to show signs of fatigue, evidenced by the increasing amount of stimulation required to complete the tracking objective (see Figs. 4, 6, 8, and 10). Because FES nonselectively recruits muscle fibers, closed-loop control offers one solution to compensate for the effect of fatigue. To reduce fatigue, the developed controller could have been implemented using an asynchronous stimulation pattern as in [62], but compensating for fatigue remains an outstanding challenge in the use of FES [48]. Likewise, while results, such as [63], [64], offer inroads to compensating for neuromuscular delays, including such methods in more complex switched systems required for coordinating limb movements, also remains an open challenge.

It is important to note that the saturation of the stimulation input (i.e., the cadence controller) does not compromise the performance of the admittance controller. Regardless of saturation, the admittance controller applied to the cycle's motors asymptotically tracks the admittance error system for all time. Because of the admittance filter, if the rider's muscles are unable to produce the desired interaction torque per the applied stimulation, the cycle decelerates to accommodate the rider and enters the assist-as-needed modality. By manipulating the desired interaction torque and the parameters in (10), the cycle's performance can be drastically changed; the interested reader can refer to [32] for additional details. Whether the participant was able-bodied (P1), had an NC with no asymmetry (P2/P4), or had an NC with asymmetry (P3), the combined cadence-admittance controllers applied to the split-crank FES cycle illustrated stable performance with adaptation, improving the tracking results and reducing oscillations (i.e., the standard deviation). Although three participants possessed unique NCs, the results indicate the developed controllers are capable of catering to a variety of NCs in their ability to evoke desired behavior from the cycle and rider. Hence, heuristic arguments are presented, which can potentially improve rehabilitation options across a spectrum of capabilities. The split-crank FES cycle offers a novel method to potentially treat and manage movement disorders, with particular emphasis on asymmetries or hemiparesis while preserving rider safety.

VI. CONCLUSION

An adaptive admitting split-crank FES cycle was successfully developed for use with individuals with movement disorders needing rehabilitation. The FES cycle is an example of a rehabilitation robot and showcases physical human–robot interaction while ensuring human safety and comfort. A combined Lyapunov-passivity-based switched systems stability analysis was presented to prove the global asymptotic stability of the admittance error system and passivity of the cadence error system with respect to the cycle. Experiments were conducted on one able-bodied participant and three participants with movement disorders. Without volition, the controllers demonstrated an average admittance tracking error of -0.13 ± 1.77 RPM with adaptation enabled and -0.03 ± 4.05 RPM with adaptation disabled across both sides of the split-crank FES cycle. With rider volition included on one participant, the average admittance tracking error was -0.10 ± 2.15 RPM, and the cycle maintained stable tracking performance. To validate the control approach and determine any rehabilitative benefits, future works will include additional investigations using a larger subject cohort. Additional protocols will also be investigated to determine which trajectories should be used to treat asymmetric disorders. While customizable, the admitted trajectory for this article was generated by averaging the capabilities of both legs such that both sides of the cycle operate at the same cadence while keeping the pedals at $180°$ of phase difference to promote symmetry training. By integrating adaptive closed-loop control with rehabilitation robots, uncertain time-varying characteristics about the FES cycle and rider are addressed, and accurate regulation of the cycle's performance is accomplished. With proper control techniques, rehabilitation goals can be explicitly designed and measured, ultimately resulting in improvements in the quality of life of those individuals affected by movement disorders.

REFERENCES

[1] S. E. Wallace and M. L. Kimbarow, *Cognitive Communication Disorders*. San Diego, CA, USA: Plural Publishing, 2016.

[2] E. J. Benjamin *et al.*, "Heart disease and stroke statistics—2017 update," *Circulation*, vol. 135, no. 10, pp. 146–603, 2017.

[3] "Spinal cord injury (SCI) 2016 facts and figures at a glance," *J. Spinal Cord Med.*, vol. 39, no. 4, pp. 493–494, 2016.

[4] J. Mackay, *The Atlas of Heart Disease and Stroke*, vol. 5. Geneva, Switzerland: World Health Organization, 2004.

[5] M. Bélanger, R. B. Stein, G. D. Wheeler, T. Gordon, and B. Leduc, "Electrical stimulation: Can it increase muscle strength and reverse osteopenia in spinal cord injured individuals?" *Arch. Phys. Med. Rehabil.*, vol. 81, no. 8, pp. 1090–1098, Aug. 2000.

[6] S. Ferrante, A. Pedrocchi, G. Ferrigno, and F. Molteni, "Cycling induced by functional electrical stimulation improves the muscular strength and the motor control of individuals with post-acute stroke," *Eur. J. Phys. Rehabil. Med.*, vol. 44, no. 2, pp. 159–167, 2008.

[7] C. Patten, J. Dozono, S. G. Schmidt, M. E. Jue, and P. S. Lum, "Combined functional task practice and dynamic high intensity resistance training promotes recovery of upper-extremity motor function in post-stroke hemiparesis: A case study," *J. Neurol. Phys. Therapy*, vol. 30, no. 3, pp. 99–115, Sep. 2006.

[8] J. Stein, H. I. Krebs, W. R. Frontera, S. E. Fasoli, R. Hughes, and N. Hogan, "Comparison of two techniques of robot-aided upper limb exercise training after stroke," *Amer. J. Phys. Med. Rehabil.*, vol. 83, no. 9, pp. 720–728, Sep. 2004.

[9] R. J. Downey, M. Merad, E. J. Gonzalez, and W. E. Dixon, "The time-varying nature of electromechanical delay and muscle control effectiveness in response to stimulation-induced fatigue," *IEEE Trans. Neural Syst. Rehabil. Eng.*, vol. 25, no. 9, pp. 1397–1408, Sep. 2017.

[10] M. Kimmel and S. Hirche, "Invariance control for safe human–robot interaction in dynamic environments," *IEEE Trans. Robot.*, vol. 33, no. 6, pp. 1327–1342, Dec. 2017.

[11] J. Zhang and C. C. Cheah, "Passivity and stability of human–robot interaction control for upper-limb rehabilitation robots," *IEEE Trans. Robot.*, vol. 31, no. 2, pp. 233–245, Apr. 2015.

[12] A. U. Pehlivan, D. P. Losey, and M. K. OMalley, "Minimal assist-as-needed controller for upper limb robotic rehabilitation," *IEEE Trans. Robot.*, vol. 32, no. 1, pp. 113–124, Feb. 2016.

[13] N. Vitiello *et al.*, "NEUROExos: A powered elbow exoskeleton for physical rehabilitation," *IEEE Trans. Robot.*, vol. 29, no. 1, pp. 220–235, Feb. 2013.

[14] S. F. Atashzar, I. G. Polushin, and R. V. Patel, "A small-gain approach for nonpassive bilateral telerobotic rehabilitation: Stability analysis and controller synthesis," *IEEE Trans. Robot.*, vol. 33, no. 1, pp. 49–66, Feb. 2017.

[15] N. Hogan, "Impedance control: An approach to manipulation: Part I-theory, part II-implementation, part III-applications," *J. Dyn. Syst., Meas., Control*, vol. 107, no. 1, pp. 1–24, Mar. 1985.

[16] Y. Li, S. S. Ge, and C. Yang, "Learning impedance control for physical robot–environment interaction," *Int. J. Control*, vol. 85, no. 2, pp. 182–193, Feb. 2012.

[17] Y. Li and S. S. Ge, "Impedance learning for robots interacting with unknown environments," *IEEE Trans. Control Syst. Technol.*, vol. 22, no. 4, pp. 1422–1432, Jul. 2014.

[18] I. Ranatunga, F. L. Lewis, D. O. Popa, and S. M. Tousif, "Adaptive admittance control for human–robot interaction using model reference design and adaptive inverse filtering," *IEEE Trans. Control Syst. Technol.*, vol. 25, no. 1, pp. 278–285, Jan. 2017.

[19] A. Roy *et al.*, "Robot-aided neurorehabilitation: A novel robot for ankle rehabilitation," *IEEE Trans. Robot.*, vol. 25, no. 3, pp. 569–582, Jun. 2009.

[20] Y. Choi, J. Gordon, D. Kim, and N. Schweighofer, "An adaptive automated robotic task-practice system for rehabilitation of arm functions after stroke," *IEEE Trans. Robot.*, vol. 25, no. 3, pp. 556–568, Jun. 2009.

[21] F. Anaya, P. Thangavel, and H. Yu, "Hybrid FES–robotic gait rehabilitation technologies: A review on mechanical design, actuation, and control strategies," *Int. J. Intell. Robot. Appl.*, vol. 2, no. 1, pp. 1–28, Mar. 2018.

[22] A. J. Del-Ama, Á. Gil-Agudo, J. L. Pons, and J. C. Moreno, "Hybrid FES-robot cooperative control of ambulatory gait rehabilitation exoskeleton," *J. Neuroeng. Rehabil.*, vol. 11, no. 1, p. 27, 2014.

[23] A. Alamdari, R. Haghighi, and V. Krovi, "Stiffness modulation in an elastic articulated-cable leg-orthosis emulator: Theory and experiment," *IEEE Trans. Robot.*, vol. 34, no. 5, pp. 1266–1279, Oct. 2018.

[24] S. A. Bowyer and F. R. Y. Baena, "Dissipative control for physical human–robot interaction," *IEEE Trans. Robot.*, vol. 31, no. 6, pp. 1281–1293, Dec. 2015.

[25] N. Alibeji, N. Kirsch, and N. Sharma, "An adaptive low-dimensional control to compensate for actuator redundancy and FES-induced muscle fatigue in a hybrid neuroprosthesis," *Control Eng. Pract.*, vol. 59, pp. 204–219, Feb. 2017.

[26] N. A. Alibeji, V. Molazadeh, B. E. Dicianno, and N. Sharma, "A control scheme that uses dynamic postural synergies to coordinate a hybrid walking neuroprosthesis: Theory and experiments," *Frontiers Neurosci.*, vol. 12, p. 159, Apr. 2018.

[27] M. J. Bellman, R. J. Downey, A. Parikh, and W. E. Dixon, "Automatic control of cycling induced by functional electrical stimulation with electric motor assistance," *IEEE Trans. Autom. Sci. Eng.*, vol. 14, no. 2, pp. 1225–1234, Apr. 2017.

[28] C. A. Cousin, V. H. Duenas, C. A. Rouse, and W. E. Dixon, "Motorized functional electrical stimulation for torque and cadence tracking: A switched Lyapunov approach," in *Proc. IEEE 56th Annu. Conf. Decis. Control (CDC)*, Dec. 2017, pp. 5900–5905.

[29] V. H. Duenas, C. A. Cousin, V. Ghanbari, and W. E. Dixon, "Passivity-based learning control for torque and cadence tracking in functional electrical stimulation (FES) induced cycling," in *Proc. Annu. Amer. Control Conf. (ACC)*, Jun. 2018, pp. 3726–3731.

[30] C. A. Cousin *et al.*, "Closed-loop cadence and instantaneous power control on a motorized functional electrical stimulation cycle," *IEEE Trans. Control Syst. Technol.*, vol. 28, no. 6, pp. 2276–2291, Nov. 2020.

[31] C. Cousin, V. H. Duenas, C. Rouse, and W. E. Dixon, "Stable cadence tracking of admitting functional electrical stimulation cycle," in *Proc. ASME Dyn. Syst. Control Conf.*, 2018, pp. 1–7.

[32] C. A. Cousin, V. Duenas, C. Rouse, and W. E. Dixon, "Admittance control of motorized functional electrical stimulation cycle," in *Proc. IFAC Conf. Cyber. Phys. Hum. Syst.*, 2018, pp. 328–333.

[33] C. A. Cousin, V. H. Duenas, C. A. Rouse, and W. E. Dixon, "Cadence and admittance control of a motorized functional electrical stimulation cycle," in *Proc. IEEE Conf. Decis. Control (CDC)*, Dec. 2018, pp. 6470–6475.

[34] C. A. Cousin, C. A. Rouse, V. H. Duenas, and W. E. Dixon, "Controlling the cadence and admittance of a functional electrical stimulation cycle," *IEEE Trans. Neural Syst. Rehabil. Eng.*, vol. 27, no. 6, pp. 1181–1192, Jun. 2019.

[35] E. Ambrosini, S. Ferrante, G. Ferrigno, F. Molteni, and A. Pedrocchi, "Cycling induced by electrical stimulation improves muscle activation and symmetry during pedaling in hemiparetic patients," *IEEE Trans. Neural Syst. Rehabil. Eng.*, vol. 20, no. 3, pp. 320–330, May 2012.

[36] E. Ambrosini, S. Ferrante, T. Schauer, G. Ferrigno, F. Molteni, and A. Pedrocchi, "Design of a symmetry controller for cycling induced by electrical stimulation: Preliminary results on post-acute stroke patients," *Artif. Organs*, vol. 34, no. 8, pp. 663–667, Aug. 2010.

[37] M. Van der Loos, L. Worthen-Chaudhari, and D. Schwandt, "A split-crank bicycle ergometer uses servomotors to provide programmable pedal forces for studies in human biomechanics," *IEEE Trans. Neural Syst. Rehabil. Eng.*, vol. 18, no. 4, pp. 52–445, Apr. 2010.

[38] L. Ting, S. Kautz, D. Brown, and F. Zajac, "Contralateral movement and extensor force generation alter flexion phase muscle coordination in pedaling," *J. Neurophysiol.*, vol. 83, no. 6, pp. 65–3351, Jun. 2000.

[39] S. J. Elmer, J. McDaniel, and J. C. Martin, "Biomechanics of counterweighted one-legged cycling," *J. Appl. Biomech.*, vol. 32, no. 1, pp. 78–85, 2016.

[40] T. C. Bulea, C. J. Stanley, and D. L. Damiano, "Part 2: Adaptation of gait kinematics in unilateral cerebral palsy demonstrates preserved independent neural control of each limb," *Frontiers Hum. Neurosci.*, vol. 11, p. 50, Feb. 2017.

[41] D. S. Reisman, A. J. Bastian, and S. M. Morton, "Neurophysiologic and rehabilitation insights from the split-belt and other locomotor adaptation paradigms," *Phys. Therapy*, vol. 90, no. 2, pp. 187–195, Feb. 2010.

[42] A. L. Penko, J. R. Hirsch, C. Voelcker-Rehage, P. E. Martin, G. Blackburn, and J. L. Alberts, "Asymmetrical pedaling patterns in Parkinson's disease patients," *Clin. Biomech.*, vol. 29, no. 10, pp. 1089–1094, Dec. 2014.

[43] D. Liberzon, *Switching in Systems and Control*. Basel, Switzerland: Birkhauser, 2003.

[44] V. H. Duenas, C. A. Cousin, C. Rouse, E. J. Fox, and W. E. Dixon, "Distributed repetitive learning control for cooperative cadence tracking in functional electrical stimulation cycling," *IEEE Trans. Cybern.*, vol. 50, no. 3, pp. 1084–1095, Mar. 2020.

[45] N. A. Kirsch, X. Bao, N. A. Alibeji, B. E. Dicianno, and N. Sharma, "Model-based dynamic control allocation in a hybrid neuroprosthesis," *IEEE Trans. Neural Syst. Rehabil. Eng.*, vol. 26, no. 1, pp. 224–232, Jan. 2018.

[46] C. Fornusek and G. Davis, "Maximizing muscle force via low-cadence functional electrical stimulation cycling," *J. Rehabil. Med.*, vol. 36, no. 5, pp. 232–237, Sep. 2004.

[47] M. Bellman, "Control of cycling induced by functional electrical stimulation: A switched systems theory approach," Ph.D. dissertation, Dept. Mech. Aerosp. Eng., Univ. Florida, Gainesville, FL, USA, 2015.

[48] D. B. Popović, "Advances in functional electrical stimulation," *J. Electromyogr. Kinesiol.*, vol. 24, no. 6, pp. 795–802, Dec. 2014.

[49] M. Ferrarin, F. Palazzo, R. Riener, and J. Quintern, "Model-based control of FES-induced single joint movements," *IEEE Trans. Neural Syst. Rehabil. Eng.*, vol. 9, no. 3, pp. 245–257, Sep. 2001.

[50] H. K. Khalil, *Nonlinear Systems*, 3rd ed. Upper Saddle River, NJ, USA: Prentice-Hall, 2002.

[51] W. E. Dixon, A. Behal, D. M. Dawson, and S. Nagarkatti, *Nonlinear Control of Engineering Systems: A Lyapunov-Based Approach*. Boston, MA, USA: Birkhauser, 2003.

[52] A. F. Filippov, "Differential equations with discontinuous right-hand side," in *Fifteen Papers on Differential Equations* (American Mathematical Society Translations: Series 2), vol. 42. Providence, RI, USA: American Mathematical Society, 1964, pp. 199–231.

[53] B. Paden and S. Sastry, "A calculus for computing Filippov's differential inclusion with application to the variable structure control of robot manipulators," *IEEE Trans. Circuits Syst.*, vol. 34, no. 1, pp. 73–82, Jan. 1987.

[54] R. Kamalapurkar, J. A. Rosenfeld, A. Parikh, A. R. Teel, and W. E. Dixon, "Invariance-like results for nonautonomous switched systems," *IEEE Trans. Autom. Control*, vol. 64, no. 2, pp. 614–627, Feb. 2019.

[55] K. J. Hunt *et al.*, "Control strategies for integration of electric motor assist and functional electrical stimulation in paraplegic cycling: Utility for exercise testing and mobile cycling," *IEEE Trans. Neural Syst. Rehabil. Eng.*, vol. 12, no. 1, pp. 89–101, Mar. 2004.

[56] M. O. Ibitoye, N. A. Hamzaid, N. Hasnan, A. K. A. Wahab, and G. M. Davis, "Strategies for rapid muscle fatigue reduction during FES exercise in individuals with spinal cord injury: A systematic review," *PLoS ONE*, vol. 11, no. 2, Feb. 2016, Art. no. e0149024.

[57] N. Stefanovic, M. Ding, and L. Pavel, "An application of nonlinear control and gain scheduling to erbium doped fiber amplifiers," *Control Eng. Pract.*, vol. 15, no. 9, pp. 1107–1117, Sep. 2007.

[58] T. Fujinaka, Y. Kishida, M. Yoshioka, and S. Omatu, "Stabilization of double inverted pendulum with self-tuning neuro-PID," in *Proc. IEEE-INNS-ENNS Int. Joint Conf. Neural Netw.*, vol. 4, Jul. 2000, pp. 345–348.

[59] F. Nagata, K. Kuribayashi, K. Kiguchi, and K. Watanabe, "Simulation of fine gain tuning using genetic algorithms for model-based robotic servo controllers," in *Proc. Int. Symp. Comput. Intell. Robot. Automat.*, Jun. 2007, pp. 196–201.

[60] N. J. Killingsworth and M. Krstić, "PID tuning using extremum seeking: Online, model-free performance optimization," *IEEE Control Syst. Mag.*, vol. 26, no. 1, pp. 70–79, Feb. 2006.

[61] R. Kelly, V. Santibáñez, and J. Loría, *Control of Robot Manipulators in Joint Space*. Berlin, Germany: Springer, 2006.

[62] R. J. Downey, E. Ambrosini, S. Ferrante, A. Pedrocchi, W. E. Dixon, and G. Ferrigno, "Asynchronous stimulation with an electrode array reduces muscle fatigue during FES cycling," in *Proc. Int. Func. Elect. Stimul. Soc.*, Banff, AB, Canada, Sep. 2012, pp. 154–157.

[63] R. Kamalapurkar, N. Fischer, S. Obuz, and W. E. Dixon, "Time-varying input and state delay compensation for uncertain nonlinear systems," *IEEE Trans. Autom. Control*, vol. 61, no. 3, pp. 834–839, Mar. 2016.

[64] S. Obuz, J. R. Klotz, R. Kamalapurkar, and W. Dixon, "Unknown time-varying input delay compensation for uncertain nonlinear systems," *Automatica*, vol. 76, pp. 222–229, Feb. 2017.
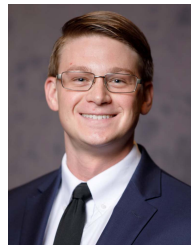
Christian A. Cousin (Member, IEEE) received the Ph.D. degree in mechanical engineering from the University of Florida, Gainesville, FL, USA, in 2019.

He joined as a Faculty Member with the Department of Mechanical Engineering, The University of Alabama, Tuscaloosa, AL, USA, in 2019. He received the National Science Foundation Graduate Research Fellowship in the spring of 2016. His research interests include nonlinear and adaptive control, switched and hybrid systems, cyber-physical systems, hybrid exoskeletons, functional electrical stimulation, human–robot interaction, rehabilitation, and machine learning.

Courtney A. Rouse received the Ph.D. degree in mechanical engineering from the University of Florida, Gainesville, FL, USA, in 2019. Her dissertation was on the control of motorized functional electrical stimulation exercises for neuromuscular therapy.

She is currently a Research Engineer in intelligent systems with the Southwest Research Institute, San Antonio, TX, USA.

Dr. Rouse received the 2020 Best Dissertation Award in mechanical and aerospace engineering.

Warren E. Dixon (Fellow, IEEE) received the Ph.D. degree from the Department of Electrical and Computer Engineering, Clemson University, Clemson, SC, USA, in 2000.

He was selected as a Eugene P. Wigner Fellow and a Staff Researcher with the Oak Ridge National Laboratory, Oak Ridge, TN, USA. In 2004, he joined the Department of Mechanical and Aerospace Engineering, University of Florida, Gainesville, FL, USA, where he currently holds the Newton C. Ebaugh Professorship. His main research interest has been the development and application of Lyapunov-based control techniques for uncertain nonlinear systems.

Dr. Dixon was elected as an American Society of Mechanical Engineers (ASME) and IEEE Fellow for his contributions to adaptive control of uncertain nonlinear systems. His work has been acknowledged by various career and best paper awards.